RSC Advances

PAPER

View Article Online
View Journal | View Issue

Cite this: *RSC Adv.*, 2018, **8**, 21431

One-step topological preparation of carbon doped and coated TiO_2 hollow nanocubes for synergistically enhanced visible photodegradation activity†

Chengjiang Zhang,[a] Amin Cao,[a] Lianqing Chen, *[ab] Kangle Lv,[a] Tsunghsueh Wu[b] and Kejian Deng[a]

Various three-dimensional TiO_2 hollow structures have attracted strong scientific and technological attention due to their excellent properties. 3D hierarchical TiO_2 hollow nanocubes (TiO_2-HNBs) are not good candidates for industrial photocatalytic applications due to their large energy gap which is only activated by UV light. Herein, visible-light-responsive carbon doped and coated TiO_2-HNBs (C@TiO_2-HNBs) with a dominant exposure of {001} facets have been prepared *via* a template-engaged topotactic transformation process using facile one-step solvothermal treatment and a solution containing ethanol, glucose and $TiOF_2$. The effects of reaction time and glucose/$TiOF_2$ mass ratio on the structure and performance of C@TiO_2-HNBs were systematically studied. We found that glucose played an important role in providing H_2O during the topological transformation from self-templated $TiOF_2$ cubes into 3D hierarchical TiO_2 hollow nanocubes *versus* dehydration reactions, where its main function was as a carbon source. Coated carbon was deposited predominantly on the surface as sp^2 graphitic carbon in extended p conjugated graphite-like environments, and doped carbon mainly replaced Ti atoms in the surface lattice to form a carbonate structure. The results were confirmed using TEM SEM, EDS, XRD, FT-IR, XPS and Raman spectroscopic studies. The C@TiO_2-HNBs achieved greatly improved RhB photodegradation activity under visible light irradiation. The catalyst prepared with glucose/$TiOF_2$ at a mass ratio of 0.15 (T24-0.15) showed the highest photodegradation rate of 96% in 40 min, which is 7.0 times higher than those of the TiO_2-HNBs and P25. This new synthetic approach proposes a novel way to construct carbon hybridized 3D hierarchical TiO_2 hollow nanocubes by combining two modification methods, "element doped" and "surface sensitized", at the same time.

Received 20th March 2018
Accepted 31st May 2018

DOI: 10.1039/c8ra02427h

rsc.li/rsc-advances

1. Introduction

TiO_2 has become one of the most popular photocatalysts due to its non-toxicity, high chemical stability and environmental friendliness.[1] However, the relatively wide band gap of anatase TiO_2 (3.2 eV) severely restricts its practical applications by making it active only for ultraviolet light, a very small part (about 4%) of solar light.[2] Therefore, enhancing the visible light response of TiO_2-based photocatalysts to make full use of the most abundant amount of the solar spectra is an issue of great importance which remains a great challenge.

To date, there have been a significant amount of studies devoted to improving the visible light utilization of TiO_2 by semiconductor coupling,[3,4] metal and non-metal ion doping[5,6] and surface sensitized modification.[7,8] Although semiconductor coupling can effectively utilize heterojunction effects to speed up the separation rate of photo-generated electron–hole pairs and improve photocatalytic activity, photoactivity strongly depends on heterojunction structures and energy conversion efficiencies are too low for industrial applications.[9,10] On the other hand, carbon doping is an effective strategy which is often employed for adjusting band gaps with multi-step procedures and lattice exchange at high temperature. The carbon species surface sensitization approach can dramatically extend the light-responsive-region of TiO_2 from UV to the visible region.[11]

As a promising dopant and sensitizer, the non-metal element C has become attractive for more and more scientists due to its reduction in potential traps for electron–hole pair recombination and perfect light absorption abilities. Therefore, the fabrication of C doped TiO_2 (ref. 12) or C coated TiO_2 (ref. 13

[a]*Key Laboratory of Catalysis and Materials Science of the State Ethnic Affairs Commission & Ministry of Education, South-Central University for Nationalities, Wuhan, 430074, P. R. China. E-mail: lqchen@mail.scuec.edu.cn; Fax: +86-27-67842752; Tel: +86-27-67842752*

[b]*Department of Chemistry, University of Wisconsin-Platteville, Platteville, 53818, USA. E-mail: chenlia@uwplatt.edu*

† Electronic supplementary information (ESI) available. See DOI: 10.1039/c8ra02427h

and 14) is an effective and environmentally friendly strategy for improving the visible absorption ability of TiO_2. Unfortunately, only a few methods have been adopted to produce C doped or C coated TiO_2 nanosheets and nanorods.[15,16] There are still a few effective approaches capable of synthesizing C modified 3D TiO_2 hollow nanomaterials,[17] but the type and concentration of carbon sources can't be greatly controlled and carbon is mostly introduced onto the surface, not doped into the bulk of TiO_2 catalysts.[18] Furthermore, these methods are limited due to their complicated processes, high cost and small production scale. In spite of this, the fabrication of C modified TiO_2 catalysts has aroused great interest and to date, research on how to combine the two modification methods, "C doping" and "C surface sensitization", at the same time to modify TiO_2-based catalysts to expand their absorption ranges is far from satisfactory.

The key to this problem is to find a suitable carbon source that facilitates both modification methods for simultaneous fabrication. Glucose, an electron-donating organic molecule with a hole-trapping agent and a polyhydroxy aldehyde molecule with high carbon content, is a good candidate which has both alcohol and aldehyde properties.[19] Moreover, the low prices of raw materials also help in its application into industrial production. Therefore, glucose modified TiO_2 will play a very positive role in solving energy and ecological problems.

As we all know, C modified TiO_2 has attracted increasing interest from scientists. Doping C into TiO_2 lattices can occur either by a substitution of the anionic (O) sites (C@O) or a substitution of the cationic (Ti) sites (C@Ti). The corresponding lattice environments can be represented as Ti–C–Ti–O and C–O–Ti–O, respectively. According to theoretical calculations,[20,21] it can be found that C@O reduced the energy gap of TiO_2 by a small magnitude (0.08 eV) and also produced a gap state with the characteristics of C 2p. In comparison, C@Ti caused C 2s states to rise to just below the original conduction band, so that the calculated E_g was decreased to a value of 2.85 eV corresponding to the visible light region.[22] In the band structure, these dopant states were found to be positioned between the conduction and valence bands of pure TiO_2.[23]

It is well known that the diverse morphological changes of TiO_2 nanomaterials can be used to tune their shape-dependent physical properties. Various 3D TiO_2 hollow structures have been synthesized using different methods, such as TiO_2 hollow spheres or tubular structures constructed from nanowires, nanorods, nanosheets or nanoparticles.[24,25] However, these structures are mainly spherical-like and composed of random aggregated building blocks. The synthesis of non-spherical 3D TiO_2 hollow nanomaterials, such as cubes and boxes, composed of ordered nanosheets, still remains a great challenge. Generally, the efficiency of TiO_2-based catalysts depends on their surface area and exposed facets. To date, the relationship between their properties and high energy {001} facets has attracted an explosion of interest.[26,27] According to a density functional theory-based study, the different facets' average surface energies of anatase TiO_2 are as follows: {110} (1.09 J m^{-2}) > {001} (0.90 J m^{-2}) > {100} (0.53 J m^{-2}) > {101} (0.44 J m^{-2}).[28] Therefore, a great number of researchers try to focus on the exposure of the high surface energy facets of TiO_2 to obtain much higher chemical reactivity.[29,30]

Based on the above considerations, we tried to establish the fabrication of C doped and coated TiO_2 hollow nanocubes (C@TiO_2-HNBs) with exposed high energy {001} facets through a sample one-step topotactic transformation process with a $TiOF_2$ template using glucose as a carbon source. Herein, by using low-cost glucose, $TiOF_2$ as a self-templating raw material and varying the reaction time and glucose/$TiOF_2$ mass ratio, carbon species were successfully deposited on the surface and doped into the lattice of TiO_2-HNBs, which were assembled using six ordered nanosheets with dominant exposed {001} facets. In addition, due to their strong visible light adsorption ability and suppression of charge recombination, RhB photodegradation activity was significantly promoted under visible light irradiation. Lastly, the detection of active species, degradation stability and the probable mechanism have been discussed.

2. Experimental section

2.1. Topological synthesis process

All chemical reagents and solvents were of analytical grade quality, obtained from commercial suppliers and used directly without further purification (Wuhan Guoyao Chemical Reagent Co. Ltd.). Doubly distilled water was used throughout all experiments.

Firstly, the $TiOF_2$ precursor was prepared as the nanocubic template according to a previously reported procedure.[31,32] In a typical procedure, 5 mL HF (AR, ≥ 40%) was slowly added dropwise into 30 mL CH_3COOH (AR, ≥ 99.5%) under continuous magnetic stirring. After stirring for 0.5 h, the mixed solution was added to a polyvinyl fluoride beaker containing 15 g tetrabutyl titanate (TBT, CP, ≥ 98.0%) to obtain a white emulsion. This was then transferred to a dry 100 mL Teflon-lined autoclave and the reaction was maintained at 200 °C for 12 h. After being cooled to 25 °C, the precipitate was filtered through a microporous organic filtration membrane (0.4 μm) and washed with absolute ethanol (AR, ≥ 99.7%) and distilled water, then dried at 120 °C for 6 hours. Finally, the white $TiOF_2$ precursor was obtained.

Secondly, using the $TiOF_2$ as a precursor,[33] ethanol as a solvent and glucose (AR, ≥ 99.0%) as a carbon source, carbon doped and coated 3D hierarchical TiO_2 hollow nanocubes (C@TiO_2-HNBs) were synthesized *via* a template-engaged topotactic transformation process. The effects of reaction time and glucose/$TiOF_2$ mass ratio on the structure of C@TiO_2-HNBs were systematically studied.

The C@TiO_2-HNB samples were prepared at different reaction times: typically, 0.1 g of anhydrous glucose and 1 g of $TiOF_2$ (mass ratio of 0.1/1) were added to a high-pressure reactor containing 40 mL anhydrous ethanol for ultrasonic dispersion for 30 min, then maintained at 200 °C for 24 h. After cooling to 25 °C, the mixture was vigorously shaken and allowed to sit still for 3 h until the precipitate was completely settled. The precipitate was then filtered through a microporous organic filtration membrane (0.4 μm). To eliminate the surface

adsorbed fluoride ions, the precipitate was washed using 0.1 M NaOH, followed by distilled water until the pH value of the filtrate was about 7. It was then dried and triturated with a small amount of absolute ethanol to obtain a light black powder product. The obtained product was named T-24, where 24 represents the reaction time. The above steps remained unchanged and the reaction time varied between 12 h, 18 h, 36 h and 48 h to find the optimal time. These products were recorded as T-12, T-18, T-36 and T-48, respectively.

The C@TiO_2-HNB samples were also prepared at different glucose/$TiOF_2$ mass ratios: in a typical synthesis, 0.05 g of anhydrous glucose and 1 g of $TiOF_2$ (mass ratio of 0.05/1) were added to a high-pressure reactor containing 40 mL anhydrous ethanol for ultrasonic dispersion for 30 min, then reacted at 200 °C for 24 h. After the end of the reaction, the rest of the steps were the same as above and the final product was recorded as T24-0.05. The optimal mass ratio was expected to be found within 0/1, 0.1/1, 0.15/1, 0.2/1 and 0.25/1. The resulting products were respectively recorded as TiO_2-HNBs T24-0.1, T24-0.15, T24-0.2 and T24-0.25.

2.2. Characterization

The morphology of the C@TiO_2-HNBs samples was observed using a transmission electron microscope (TEM) (Tecnai G^2 20, USA) with an acceleration voltage of 200 kV. Scanning electron microscopy (SEM) images were obtained on a field emission scanning electron microscope (Hitachi, Japan). X-ray diffraction (XRD) patterns were obtained using a D8-advance X-ray diffractometer (Bruker, German) with Cu K_α radiation at a scan rate of 0.02° 2θ s^{-1}. The accelerated voltage and applied current were 40 kV and 80 mA, respectively. The infrared spectra (IR) of these samples were obtained using Fourier transform infrared spectroscopy (Nexus 470 FT-IR, Shimadzu, Japan). X-ray photo-electron spectroscopy (XPS) measurements were performed using a Kratos XSAM800 XPS system with Mg K_α radiation and a charge neutralizer; all of the binding energies were referenced to the C 1s peak at 284.8 eV of the surface adventitious carbon. Raman spectra were used to characterize the optical properties and were obtained using a DXR Smart Raman Spectrometer (Thermo, USA). A UV2600UV-vis spectrophotometer (Shimadzu, Japan) was used for UV-vis diffuse reflectance spectroscopy (DRS) and $BaSO_4$ was used as the reference sample. Photoluminescence (PL) spectra were recorded using an F-7000 Fluorescence Spectrophotometer (Hitachi, Japan).

2.3. Photocatalytic measurements

The photocatalytic activity of the as-prepared C@TiO_2-HNBs was evaluated using the organic dye RhB (1 g L^{-1}) as the target pollutant. The specific process was as follows: RhB solution was prepared at an initial concentration of 5×10^{-4} mol L^{-1} (pH = 7–8), and transferred to an Erlenmeyer flask with 50 mg catalyst by ultrasound dispersion. The reaction mixture was stirred to reach adsorption equilibrium in the dark overnight. The mixture was transferred to a photoreaction bottle, which had double glass and a magnet for stirring. A 210 W Xe lamp, equipped with an ultraviolet cutoff filter, served as the visible light source. The distance between the photoreaction bottle and the light source was 20 cm. Samples were taken at set time intervals, and each time 3.5 mL was centrifuged to measure the absorbance of the upper liquid. UV-vis absorption spectra were measured at different intervals to monitor the reaction. All of the measurements were carried out at room temperature.

The photocatalytic activity of the C@TiO_2-HNBs samples was evaluated using a photoluminescence (PL) technique with coumarin as a probe molecule, which readily reacted with ˙OH radicals to produce a highly fluorescent product, 7-hydroxycoumarin.[34] TiO_2 and water react to form the active species hydroxyl radical (˙OH), and then coumarin rapidly binds with the hydroxyl radicals to generate 7-hydroxycoumarin, which has strong fluorescence properties (as shown in ESI Scheme S1†). The external conditions for the detection of active species (˙OH) is consistent with the photodegradation rate of RhB. The specific process is as follows: the suspension of TiO_2 (1.0 g L^{-1}) containing coumarin (0.1 mmol L^{-1}) was mixed under magnetic stirring, and was then shaken overnight. The mixture was irradiated with a 210 W xenon lamp light and samples were taken at set 2 minute intervals. The solution was filtered through a microporous organic filtration membrane (0.22 μm). The fluorescence spectrophotometer was used to analyze filtrate using excitation at a wavelength of 334 nm.

3. Results and discussion

3.1. Tuning the morphology of the as-synthesized catalysts using different parameters

Fig. S1† shows TEM images of the as-synthesized samples of $TiOF_2$, TiO_2-HNBs and C@TiO_2-HNBs (Glu/$TiOF_2$ mass ratio = 0.1/1) obtained by varying the hydrothermal reaction time at 200 °C. Fig. S1(a)† shows that $TiOF_2$ consists of uniform smooth surface solid nanocubes of about 250 nm. For comparison, Fig. S1(b)† indicates 3D TiO_2 hollow nanocubes (TiO_2-HNBs) with a Glu/$TiOF_2$ mass ratio of 0. It was found that their size was comparable to that of $TiOF_2$ and they were composed of six facets tiled with large surface nanosheets.[35] Fig. S1(d–h)† are as-prepared carbon modified TiO_2 hollow nanocubes at different reaction times. Fig. S1(d)† shows that the T-12 sample did not completely transform from a nanocube into a hollow box. The solid structure is ascribed to the short reaction time and incomplete conversion of $TiOF_2$ to TiO_2. All of the samples with glucose exhibited well-shaped hollow nanocube assembly by nanosheets when the time was increased to 18 h and above. It was obviously observed that there was a certain amount of black hairy tentacles on the surfaces of the hollow boxes, confirming that carbon was accumulated on the surface of the TiO_2-HNBs.

Fig. 1 exhibits SEM images of the as-synthesized samples obtained by hydrothermal reactions at different reaction times. Fig. 1(a and b) shows the uniform solid cubes of $TiOF_2$ and completely 3D TiO_2 hollow boxes. Fig. 1(c–g) exhibits the hollow boxes of C@TiO_2-HNBs at different reaction times. As shown in Fig. 1(c–g), the hollow box structures are very obvious and uniform and there are many hairy tentacles on the surfaces of TiO_2 hollow boxes, especially at the fracture, meaning that carbon was deposited on the surface of the TiO_2 hollow boxes

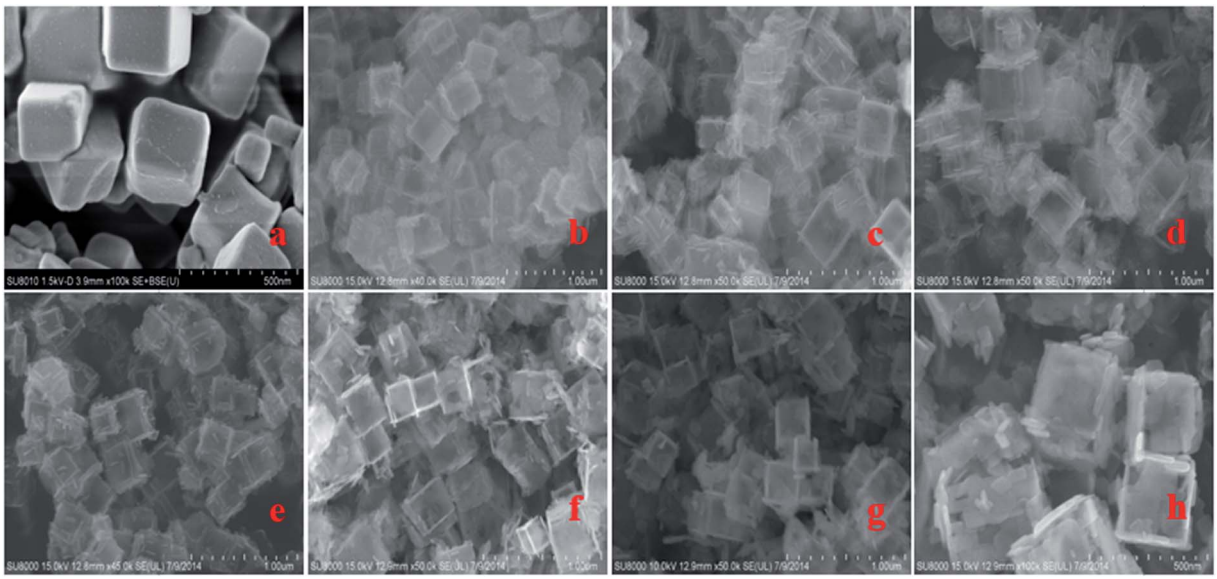

Fig. 1 SEM images of the as-synthesized catalysts at different reaction times: (a) $TiOF_2$, (b) TiO_2-HNBs, (c) T-12, (d) T-18, (e) T-24, (f) T-36, (g) and (h) T-48.

successfully. When the reaction time was increased up to 48 h, the hollow boxes became broken. Considering the energy consumption problem, 24 hours was chosen as the optimal time. The results of SEM are well consistent with those of TEM.

Fig. S2† displays TEM images of the as-prepared catalysts obtained with varying mass ratios of Glu/$TiOF_2$ at 200 °C for 24 h. As Fig. S2† shows, the morphology of the TiO_2 hollow nanocubes did not change significantly and remained as uniform 3D hollow boxes with a particle size of ~280 nm after the addition of different amounts of glucose. As the amount of glucose increased in Fig. S2(a–e),† most of the hollow nanocubes had a relatively homogeneous layer of coated carbon on the surface, and the hollow box-like structure of TiO_2 began to agglomerate and collapse gradually. HRTEM images (see Fig. S2f†) were obtained to confirm that the lattice spacing was about 0.235 nm, which is in good agreement with the {001} crystallite facet of anatase titanium dioxide. Unlike previously reported TiO_2 spherical hollow structures, the as-prepared TiO_2 nanocubes exhibited 3D hierarchical hollow nanocube structures consisting of six ordered dominant exposed {001} facet nanosheets.

Fig. 2 shows SEM images of the as-prepared catalysts obtained by hydrothermal reactions with different mass ratios of Glu/$TiOF_2$ at 200 °C for 24 h. Fig. 2(a–c and e) show a very complete and uniform hollow box structure which corresponds to those shown in the TEM images, whereas Fig. 2(e) shows severe disintegration and agglomeration which might be caused by excessive –OH and –CHO groups in the glucose molecules. With increases in the amounts of glucose added, the dehydration reaction didn't completely happen, and then there were a great deal of –OH and –CHO groups left. The –OH from glucose and TiO_2 can form the surface Ti–O–C bond at high temperature, and the –CHO in glucose can combine with –OH on the TiO_2 surface and form a O=C–O–Ti structure, causing the hollow nanocubes to gradually agglomerate, break and collapse. An enlarged image of sample T24-0.1 (see Fig. 2(f)) was obtained to confirm the complete morphology of the hollow nanocubes. Even after calcination, the morphology was very stable according to our other reports.[36]

Fig. S3† shows EDS images of sample T24-0.15. From the EDS scan maps it can be seen that there were Ti, O and C elements in the catalyst, of which the Ti and O elements are distributed uniformly. However, the conductive paste is the sample carrier, and the conductive paste is mainly composed of C element, which leads to the distribution of the edge C in the C element diagram. However, the presence of C in the region of the T24-0.15 sample is mainly due to the distribution of the carbon doped and coated TiO_2 semiconductor with glucose in the experiment. The shapes of the three elements in these maps and the SEM images are very similar. In addition, the scanning of the red square frame in the SEM image of Fig. S3† was performed by elemental point sweep. From the point-sweep graph and the data analysis, it was found that the atomic abundance of Ti and O elements satisfies the molar ratio of its molecular formula, which can be seen from the data in Table 1. The elemental percentages of Ti and O are 60.84% and 37.17%, respectively. The elemental percentage of doped and coated C is 1.99%. The peak at about 1.5 keV is ascribed to the peak of the Al element of the aluminum target as the sample stage under testing. This confirms that some carbon is accumulated on the surface. However, there is a significant amount of C in the particle, which is uniform and likely to be due to doping into the lattice of TiO_2.

The probable formation mechanism of carbon doped and coated TiO_2 hollow nanocubes (C@TiO_2-HNBs) has been proposed *via* a process of topological transformation involving template participation, as shown in Fig. 3. Ethanol was used as a solvent to provide mild reaction conditions. The dehydration

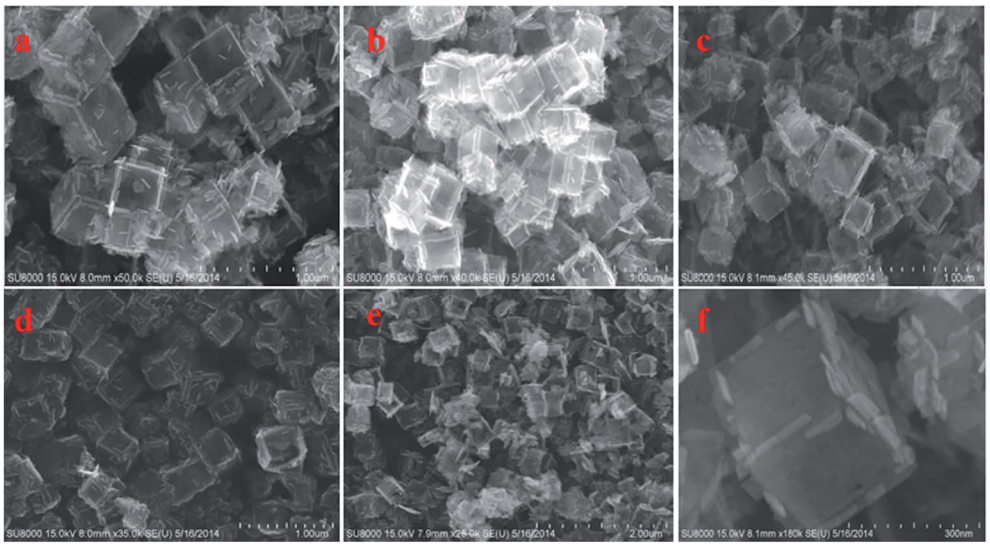

Fig. 2 SEM images of the as-prepared catalysts with different mass ratios of Glu/$TiOF_2$ at 24 h: (a) T24-0.05, (b) T24-0.1, (c and f) T24-0.15, (d) T24-0.2 and (e) T24-0.25, and (f) an enlarged image of T24-0.1.

Table 1 T24-0.15 sample EDS point-scan data

Elt.	Line	Intensity (c/s)	Atomic %	Conc wt %
C	K_α	33.12	4.56	1.99
O	K_α	213.26	58.77	37.17
Ti	K_α	1056.72	36.67	60.84

reaction of ethanol and glucose at 200 °C provided H_2O and promoted the hydrolysis of $TiOF_2$. Self-templated $TiOF_2$ cubes will transform into TiO_2 during the solvothermal reaction by the transformation of $TiOF_2$ to anatase TiO_2 nanocrystals (eqn (1)–(3)).[37] It has been reported that fluoride ions facilitate the formation of high-energy anatase TiO_2 nanosheets due to the fact that the adsorption of F^- on the surface of TiO_2 nanocrystals can sharply reduce the surface energy of the (001) facets. Therefore, it is understandable that the precursor $TiOF_2$ can transform into a TiO_2 hollow nanocube assembly from TiO_2 nanosheets with exposed high-energy (001) facets. Glucose is a polyhydroxy aldehyde molecule with a high carbon content and can easily dehydrate to generate carbon and other fragments containing –OH and –CHO groups due to the instability of the polyhydroxy and aldehyde groups. Preferentially generated carbon plays a very positive role as it favours being mainly involved in doping TiO_2. However, the dehydrated fragments containing hydroxyl and aldehyde groups are adsorbed on the surface of TiO_2 due to the formation of chemical bonds by the hydroxyl groups (surface Ti–O–C bond and O=C–O–Ti structure) on the surface of TiO_2. The dehydration reaction is further developed at 200 °C, resulting in a large amount of carbon loading (eqn (4) and (5)). As Fig. 3 shows, with the increasing addition of excess amounts of glucose, the dehydration reaction can't completely happen, and a great deal of fragments with –OH and –CHO groups are left, resulting in a small number of hollow nanocubes which gradually agglomerate, break and collapse.

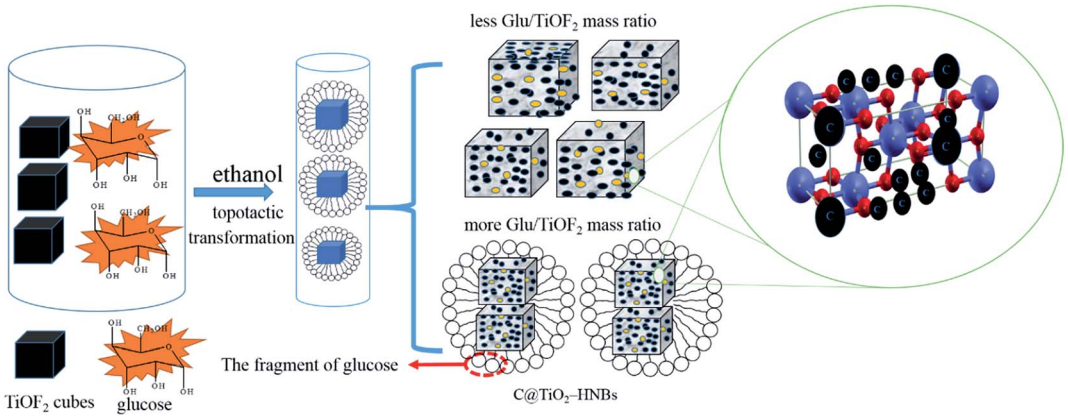

Fig. 3 The probable formation process of the 3D C@TiO_2-HNBs.

$$TiOF_2 + 2CH_3CH_2OH \rightarrow TiO_2 + 2HF + 2CH = CH_2(CH_3CH_2OCH_2CH_3)\text{alcohol} \xrightarrow{\text{dehydration}} \text{alkene (ester)} + H_2O \quad (1)$$

$$C_6H_{12}O_6 = C \text{ (doped } TiO_2) + 6H_2O + \text{glucose fragment–OH} \quad (2)$$

$$TiOF_2 + H_2O = TiO_2 \text{ (anatase)} + 2\ HF \text{ (}\textit{in situ}\text{ transformation)} \quad (3)$$

$$\text{Glucose fragment–OH} + TiO_2\text{–OH} = C \text{ (coated } TiO_2) + H_2O \quad (4)$$

$$\text{Glucose fragment–CHO} + TiO_2\text{–OH} = C \text{ (coated } TiO_2) + H_2O \quad (5)$$

3.2. Tuning the crystal planes of the as-synthesized samples

As we know, the crystal planes of catalysts play an important role in their photocatalytic properties. The XRD pattern of samples of Glu/$TiOF_2$ = 0.1/1 after 200 °C hydrothermal reaction at different reaction times is shown in Fig. 4A. In the curve of T-12, the (100), (200) and (210) crystal planes of $TiOF_2$ corresponding to $2\theta = 23.6°$, 48.1° and 54.1° were observed and the (101) (004), (200), (105) and (211) crystal planes of anatase TiO_2 corresponding to 2θ = 25.37°, 37.98°, 48.1°, 54.1° and 55.1° were obtained compared with the PDF#21-1272 standard card. This led to our conclusion that both precursor $TiOF_2$ and TiO_2 were presented in sample T-12. It was deduced that the precursor $TiOF_2$ was not fully converted to anatase TiO_2 in the topotactic transformation process with $TiOF_2$ as a template, due to the fact that 12 h hydrothermal time was too short. This is consistent with the TEM and SEM characterization. At high temperatures, when the hydrothermal time was increased from 18 h to 48 h, $TiOF_2$ was completely transformed into anatase TiO_2, and the diffraction peaks were more obvious and sharper, especially for the (105) and (211) crystal planes corresponding to 2θ = 54.1°, and 55.1°, which implied a higher degree of crystallization. Due to the F^- ions as shape control agents, no rutile patterns were formed in the as-prepared samples. With increasing hydrothermal time, the degree of crystallization of anatase TiO_2 hollow box-like structures was higher and more carbon was doped into the bulk, therefore the crystal surface of TiO_2 was better than before, which is also consistent with the corresponding TEM and SEM characterization (Table 2).

Fig. 4B shows the XRD pattern of the as-synthesized catalysts obtained after hydrothermal reactions at 200 °C for 24 h at different mass ratios of Glu/$TiOF_2$. Compared to the PDF#21-1272 standard card, the 2θ diffraction peaks of all of the as-synthesized catalysts were consistent with the characteristic peaks of anatase TiO_2. As the amount of glucose gradually increased, the shape of the diffraction peak at 2θ = 54.1° corresponding to the (105) crystal plane, exhibited a great change from sharp to flattened, which implied that after the addition of glucose, some carbon from glucose was coated on the surface of TiO_2, making it difficult to accurately determine the crystal planes of TiO_2 by X-ray powder diffraction. This is in good

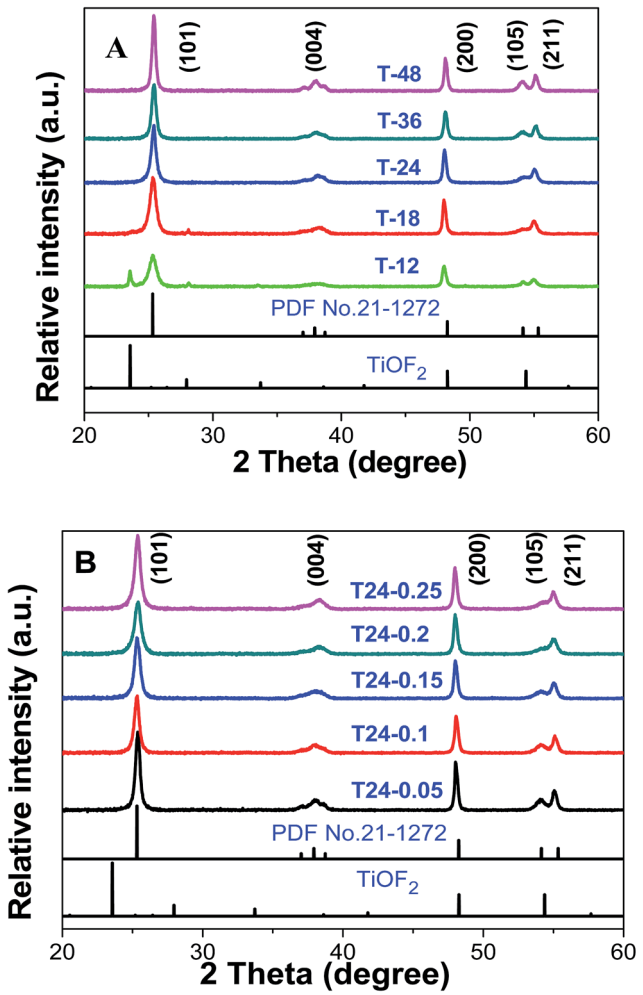

Fig. 4 The XRD pattern of the as-prepared catalyst, Glu/$TiOF_2$ = 0.1/1, (A) at different reaction times at 200 °C and (B) at different Glu/$TiOF_2$ mass ratios at 200 °C for 24 h.

agreement with the TEM and SEM results, that increasing the amount of glucose causes the morphology of the C@TiO_2-HNBs to agglomerate.

To further investigate the crystal sizes, the Scherrer equation: $D = \frac{K\lambda}{\beta \cos \theta}$ was used to calculate crystallite size based on the {101} diffraction peak. In this equation $K = 0.89$ represents the shape factor, λ represents the wavelength of X-ray irradiation (Cu Kα = 0.15418 nm), β is the full-width at half-maximum of the diffraction peak and θ is the X-ray diffraction angle. As shown in Table 1, the results indicate that the average particle sizes (about 280 nm) of various samples show little change, which corresponds to the SEM and TEM measurements. Moreover, the "*d*" space value doesn't increase, implying the unit cell dimension of the C@TiO_2-HNBs isn't likely to change during the carbon doping and coating process.

3.3. FT-IR spectra of the C@TiO_2-HNBs

As displayed in Fig. S4,† the FT-IR spectra of Glu/$TiOF_2$ = 0.1/1 reacted for different amounts of time at 200 °C (A) and at

Table 2 Structural analysis of the as-prepared samples

Sample	$XRD_{(101)}$ relative intensity (%)	$XRD_{(101)}$ peak position (°)	Crystal size[a] (nm)	*d*-spacing (Å)
T24-0.05	100	25.32	285	3.5
T24-0.1	65	25.41	283	3.5
T24-0.15	78	25.31	281	3.5
T24-0.2	68	25.37	286	3.5
T24-0.25	86	25.37	289	3.5
T18	93	25.31	290	3.5

[a] Average crystal sizes were obtained based on the {101} diffraction peak using the Scherrer equation.

varying Glu/$TiOF_2$ mass ratios at 200 °C for 24 h (B) were used to determine the carbon environments in the TiO_2 network. The stretching vibration and bending vibration of the absorption H_2O and Ti–OH groups on the surface of the samples were found at about 3444 cm^{-1}.[38] The absorption peak at 1635 cm^{-1} was ascribed to characteristic peak of the Ti–O–C–O bond, the OH characteristic peak of the TiO_2 surface was observed at 1045 cm^{-1} and a broad peak of 1087 cm^{-1} was attributed to the stretching vibration of the Ti–O–C–O bond. The stretching vibrational absorption peak of the Ti–O bond in the lattice of TiO_2 was observed at 480 cm^{-1}, and multiple peaks appeared between 450 cm^{-1} and 555 cm^{-1} due to the C substitution of Ti atoms in the TiO_2 lattice forming a Ti–O–C–O bond, implying that the doped carbon substituted Ti atoms in the lattice of TiO_2. There were two absorption peaks at 1635 cm^{-1} and 1652 cm^{-1}, which were attributed to the Ti–O–C–O bonds of TiO_2 and the O=C–O–Ti bond of the carbonate structure, respectively, further confirming that doped carbon substituted surface Ti atoms to form a carbonate structure. The characteristic absorption peak at 1393 cm^{-1} was assigned to the in-plane bending vibrational absorption peak of the C–C bond, and the peak at 2300-2350 cm^{-1} is the stretching vibration peak of the C=C bond corresponding to sp^2 carbon atoms in a disordered environment, implied that coated carbon was present in extended p conjugated graphite-like arrangements, which was confirmed by Raman analytical results.[36]

As shown in Fig. S4B,† the in-plane bending vibrational peak of C–H bond at 1343 cm^{-1} and the stretching vibration peak of the methine C–H bond at 2800-3000 cm^{-1} were significantly enhanced as the Glu/$TiOF_2$ mass ratio increased. A reasonable explanation was that more no reaction glucose fragments were left as the amount of glucose gradually increased, which is consistent with the probable formation mechanism.

3.4. Doped and coated carbon in the network of the C@TiO_2-HNBs

To further investigate the doped and coated carbon chemical environments of the as-prepared catalysts, XPS measurements of the TiO_2-HNBs and T24-0.15 samples were carried out. As shown in Fig. 5A, the three elements Ti, C and O in the C@TiO_2-HNBs were observed at the corresponding positions in the spectra. Fig. 5(B–D) displays the high-resolution XPS spectra of the corresponding elements of the T24-0.15 sample.

The high-resolution Ti 2p XPS peaks of the TiO_2 nanocubes in Fig. 5B consist of two binding energy levels of Ti $2p_{1/2}$ and $2p_{3/2}$ at 463.6 and 457.8 eV with a separation energy of about 5.80 eV; for comparison, the high-resolution Ti 2p XPS peaks of T24-0.15 consist of two binding energy levels of Ti $2p_{1/2}$ and $2p_{3/2}$ at 462.75 and 456.95 eV, respectively, with the same separation, which shifts 0.85 eV toward the lower energy region. The Ti 2p peak position differs with the nature of the carbon accumulation on the TiO_2 surface. Sample T24-0.15 shows a deviation of nearly 0.85 eV from the TiO_2-HNBs, indicative of a partial charge transfer from the surface carbon moiety to the Ti^{4+} centers in the TiO_2-HNBs network.

The O 1s XPS peaks of the TiO_2-HNBs (T24-0) and T24-0.15 (Fig. 5C) were observed at 529.75 and 529.05 eV, respectively, with a deviation energy of nearly 0.7 eV. The shifting of the lattice oxygen peak in T24-0.15 towards lower energy, relative to the TiO_2 standard, further verified the different environment due to the carbon accumulation and doping. The high-resolution XPS spectrum for O 1s (Fig. 5C1) of sample T24-0.15 showed three different environments. The energy peak positions located at 530.4, 531.6 and 532.9 eV in the C@TiO_2-HNB network are attributed to Ti–O (O^{2-} lattice oxygen), C–OH (and C–O–C) and C=O (and COO) species, respectively, implying the carbon substitution of Ti and the formation of a carbonate structure.[37,38] The enhancement of the C=O and C–OH signals in the T24-0.15 sample suggested increased hydration (H_2O and/or OH) with an increase of deposited carbon content revealed by the C 1s spectra, which was further confirmed by infrared spectra, which exhibited a C–O stretching vibration peak at 1087 cm^{-1}.

Fig. 5D shows the C 1s XPS spectra of sample T24-0.15. It can be seen that the C 1s spectra showed three distinct peaks at 284.7, 286.4 and 288.6 eV, which were due to the adventitious carbon species. The first characteristic peak at 284.7 eV was due to graphitic carbon formed on the surface of the hollow nanocubes, indicative of carbon accumulation, whereas the other two characteristic peaks (286.4 and 288.6 eV) were ascribed to C–OH (and C–O–C) and C=O (and COO) bonds, which came from carbonate-like species due to the oxidized doping carbon species. The 288.6 eV peak is a characteristic peak of C doping and exists in the form of C–O bonds, which further proved that carbon doping of the TiO_2 lattice has taken place by the substitution of Ti (C@Ti). Among the three peaks in Fig. 5D, the measured intensity of the peak due to carbonate-like features

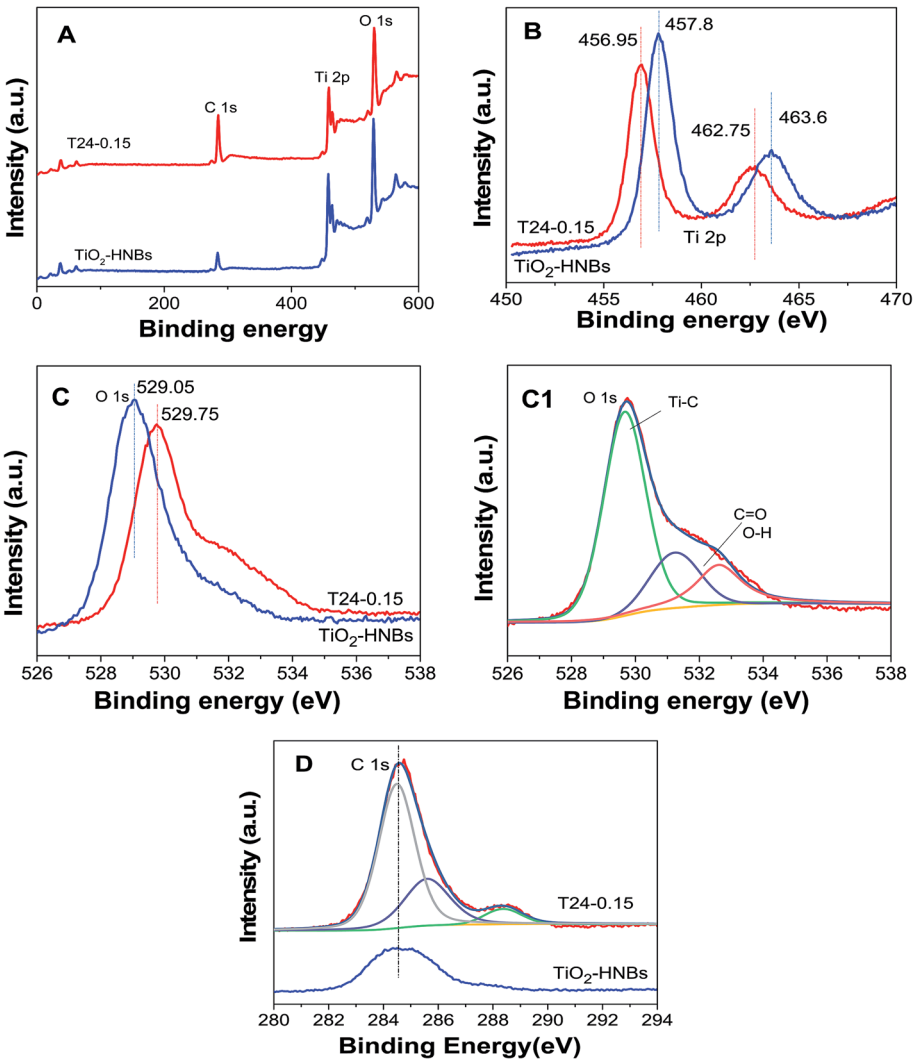

Fig. 5 XPS patterns of all types of element in the TiO_2-HNB and T24-0.15 samples.

was centered at 288.6 eV. C doping mainly replaces Ti atoms in the surface lattice to form a carbonate structure. In addition, the absence of a peak around 282.0 eV confirmed that carbon didn't substitute oxygen in the lattice, so doping may replace some Ti atoms in the Ti–O–Ti lattice to form C–O bonds. The intensity of the characteristic peak at 284.7 eV implied that the percentage of surface graphitic carbon is high and exists in the form of a C–C bond. The doped C can introduce energy states between the forbidden bands of TiO_2 and reduce the band gap to improve the absorption of visible light.

3.5. Raman spectra of the C@TiO_2-HNBs

As displayed in Fig. S5,† to further investigate carbon chemical environments the Raman spectra of samples C@TiO_2-HNBs were monitored. As we know, anatase TiO_2 exhibited six Raman active modes (three E_g, two B_{1g} and one A_{1g}). The peaks of Fig. S5A† show that these characteristic spectral features are located in the low frequency region (100–800 cm^{-1} Raman shift) of the Raman spectra for the as-prepared C@TiO_2-HNBs, which further confirms that their crystal planes belonged to the anatase phase, which is in good agreement with the XRD pattern. With different glucose concentrations, the observed peaks were similar and broadened slightly. The strong phonon peak at 145 cm^{-1} corresponding to an E_g mode shifted its position by about 5 cm^{-1} relative to anatase TiO_2, possibly due to the carbon accumulation. As the glucose/$TiOF_2$ mass ratio increased, the intensity of the lowest frequency peak at 145 cm^{-1} significantly increased, indicating the enhancement of the sample crystallinity. The other three characteristic peaks at 392, 512 and 636 cm^{-1} were well indexed to the B_{1g}, $A_{1g} + B_{1g}$, and E_g modes of anatase TiO_2, respectively.[39]

The presence and nature of carbon in the as-prepared C@TiO_2-HNBs were observed. Carbon exhibits characteristic Raman peaks in the high frequency region (see Fig. S5B†), consisting of D and G bands which could be clearly seen at around 1375 and 1588 cm^{-1}, respectively. The bands at 1375 cm^{-1} corresponded to disordered sp^2 carbon atoms originating from the graphitic (D) environment and the bands at 1588 cm^{-1} were attributed to ordered sp^2 carbon atoms in extended p conjugated graphite-like (G) arrangements. This

carbonaceous region upon deconvolution reveals that the disordered character of the D band at 1375 cm^{-1} is lower in intensity than the graphitic character of the G bands at 1588 cm^{-1}. Sample T24-0.05 showed one characteristic peak in the G band of raw graphite at 1588 cm^{-1}, which arose from the zone center E_{2g} mode, corresponding to ordered sp^2 carbon atoms. It is clear from a comparison with T24-0.25 that with increasing glucose concentration, the graphitic peak became more intense and another characteristic peak in the D band of raw graphite at 1375 cm^{-1} was also observed.

The ratio of the intensities of the D and G bands (I_D/I_G) or the degree of graphitization is an indication of the amount of graphitic carbon formed on the surface of TiO_2 hollow nanocubes; the lower the I_D/I_G ratio, the higher the degree of graphitization.[40] These values are greater than the I_D/I_G ratios (0.78–0.81) previously reported.[41] The C@TiO_2-HNB sample is therefore indicative of the presence of less graphitic carbon. As the D band is reflective of disorder and structural defects, based on I_D the disorder is likely to be decreased with increasing glucose concentration. The presence of carbon indicated that TiO_2-HNB hybrids with carbonaceous species were formed *via* hydrothermal treatment with $TiOF_2$ precursor and glucose solution.

3.6. Optical absorption of the C@TiO_2-HNBs

The UV-vis diffuse reflectance spectra of the as-prepared C@TiO_2-HNBs reacted at different reaction times (Glu/$TiOF_2$ = 0.1/1) are presented in Fig. S6A† with essentially no absorption of TiO_2 from 400 nm to 800 nm. Although TiO_2 showed an absorption onset in the UV region, the absorption of all C@TiO_2-HNBs exhibited a shoulder in the visible region. When glucose was added to samples synthesised for different amounts of reaction time, each sample had different absorptions from wavelengths of 400 nm to 800 nm, which indicated that carbon doping and coating could improve the absorption of TiO_2 in the visible region. Fig. S6B† shows the DRS pattern of the as-prepared C@TiO_2-HNBs reacted for 24 h with different Glu/$TiOF_2$ mass ratios. As can be seen from Fig. S6B,† when different amounts of glucose were added, the samples again showed different absorption at wavelengths from 400 nm to 800 nm, indicating that the amount of carbon also affected the absorption of TiO_2 in the visible region. Absorbance was enhanced with increased carbon content. According to the plot of transformed Kubelka-Munk function, the energy gaps of the TiO_2-HNBs and T24-0.15 were 2.95 eV and 2.83 eV, respectively. These values are lower than 3.2 eV, which proved that doping carbon into the TiO_2 lattice could take place by substitution of Ti (C@Ti). This is because doped carbon could form local-energy between the valence band and conduction band as the mass of glucose increased, which caused C 2s states to rise to just below the original conduction band, so that the calculated E_g was decreased to a value of 2.83 eV. This is in good agreement with previous reports.

3.7. Photocatalytic activity of the catalysts

Fig. 6A exhibits a graph of RhB degradation under simulated sunlight conditions with the as-prepared C@TiO_2-HNBs (with a Glu/$TiOF_2$ value of 0.1/1 at different reaction times. It can be seen that the degradation rate of the TiO_2-HNBs is close to 34% at 40 min, while the degradation rate of the T-24 sample reaches 90% at 40 min. The other catalyst samples also have a faster degradation rate than the TiO_2-HNBs, indicating that the visible light absorption of the TiO_2-HNBs is greatly enhanced after doping and coating with C. Fig. 6B shows a plot of RhB

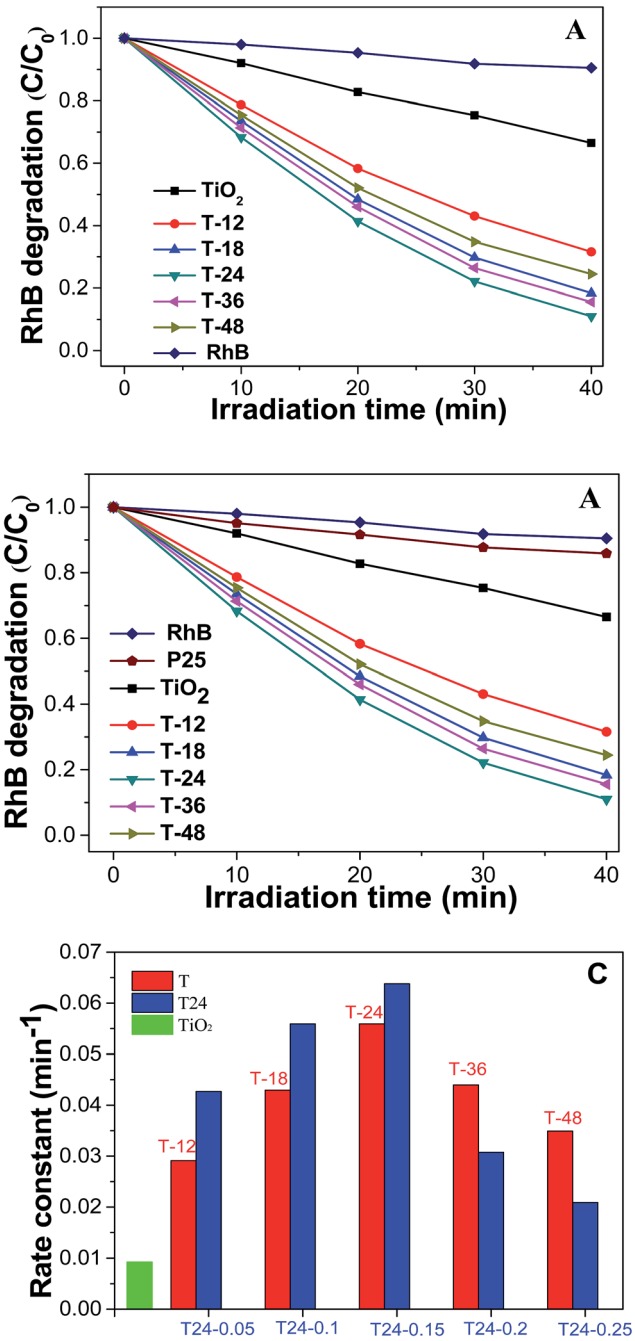

Fig. 6 The degradation of RhB by the catalysts under simulated sunlight conditions. (A) Glu/$TiOF_2$ = 0.1/1 at 200 °C different reaction times, (B) Glu/$TiOF_2$ for different mass ratios at 200 °C for 24 h and (C) a comparison of the photocatalytic degradation rate constants of the catalysts (T represents different reaction times, T24 represents different mass ratios).

degradation under Xe lamp light conditions with the as-prepared C@TiO_2-HNBs with different Glu/$TiOF_2$ mass ratios. It can be seen that the degradation rate of the T24-0.15 sample reaches 66% in about 17 min, and the degradation rate at 40 min reached as high as 96%. The degradation rate of T24-0.15 is faster than that of T24-0.25. This may be because too much C is coated, preventing the sunlight from irradiating on the surface of the TiO_2-HNBs and thus reducing the utilization of sunlight. In this process, the order of the degradation rates is T24-0.15 > T24-0.1 > T24-0.05 > T24-0.2 > T24-0.25 > TiO_2-HNBs > P25. At the same time, it can be seen from the comparison of the photocatalytic rate constants in Fig. 6C that the rates of the C doped and coated TiO_2-HNBs firstly increased and then decreased, and the photocatalytic rate of the T24-0.15 sample was 7.0 times that of the TiO_2-HNBs, while the photocatalytic rate constants of the other samples are basically larger than those of TiO_2-HNBs and P25. The above analysis could be explained by the doped C in the TiO_2 valence band introducing energy states and reducing the band gap of TiO_2. The coated C facilitates the effective separation of the electron–hole pairs generated by TiO_2-HNBs after absorbing light, thereby improving the utilization of the electron–hole pairs. However, too much doped and coated C may result in the increase of defects on the surface of the catalyst, resulting in a recombination center of electrons and holes, thereby decreasing the photocatalytic activity.

Fig. 7 displays a map of the detection of the active species of hydroxyl radicals. Fig. 7A showed the detection of hydroxyl radicals in the T24-0.15 sample. As can be seen from the figure, the fluorescence emission wavelength was 450 nm. The fluorescence intensity gradually increased, indicating that the amount of ˙OH was increasing with increased illumination time. This is because the continuously generated ˙OH and coumarin react to generate 7-hydroxycoumarin, the amount in the reaction is gradually increased, and the fluorescence intensity gradually increases.[42,43] Fig. 7B shows a linear graph of the rate of hydroxyl radical generation corresponding to as-prepared C@TiO_2-HNBs after reaction for different mass ratios of Glu/$TiOF_2$ at 200 °C. It indicates that T24-0.15 had the fastest hydroxyl radical generation rate, followed by T24-0.1, then T24-0.05, T24-0.2 and T24-0.25. The results show that T24-0.15 achieved the highest number of hydroxyl radicals generated in the same illumination time and the best photocatalytic degradation, which is consistent with the results of the photocatalytic degradation of RhB.

3.8. Photocatalyst stability

As we all know, developing TiO_2 crystals with specific facets is highly desirable in many applications for TiO_2.[44,45] In order to investigate the stability of the as-prepared C@TiO_2-HNBs, we also carried out investigations into the cycling degradation of RhB over sample T24-0.15 after washing treatment (Fig. 8). The T24-0.15 sample was recycled for 5 rounds of cyclic photocatalytic degradation experiments. As shown in the figure, as

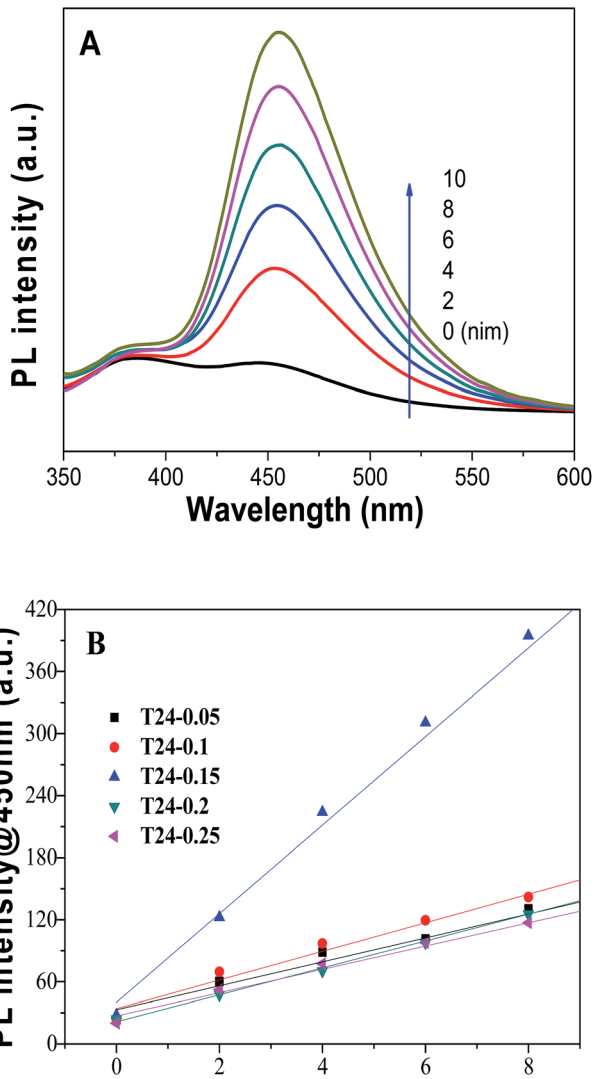

Fig. 7 The detection of active species hydroxyl radicals. (A) T24-0.15 hydroxyl radical detection and (B) a linear graph of the hydroxyl radical generation rates.

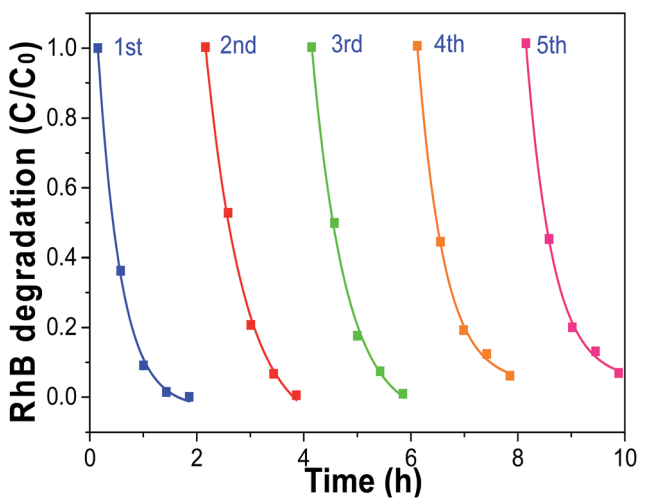

Fig. 8 Cycling degradation of RhB over sample T24-0.15 after washing under visible light irradiation.

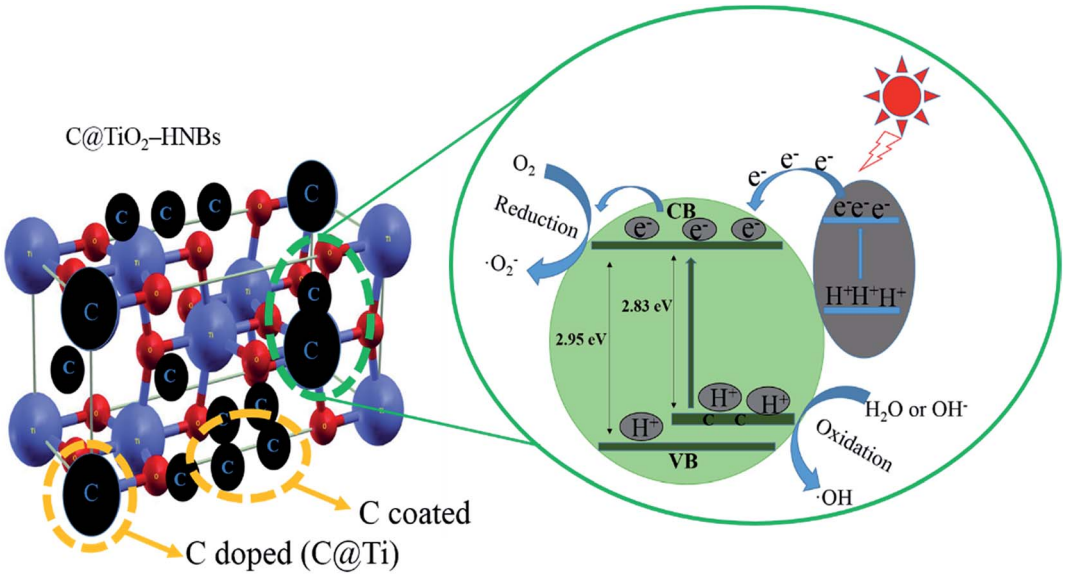

Fig. 9 Synergistically enhancing visible photocatalytic mechanism of the C@TiO_2-HNBs.

the number of photodegradation cycles increased, sample T24-0.15 still maintained high catalytic activity, indicating that the active sites on the TiO_2 surface did not decrease. In addition, it is possible that the adsorption of pollutants on surface C and the doping of C increased the number of electron transitions, and it is easier to rapidly degrade the pollutants adsorbed on the surface of C@TiO_2-HNBs, thereby not changing the surface active sites of C@TiO_2-HNBs. The results demonstrated the stable photocatalytic activity of our catalyst during the recycling process.

3.9. Probable mechanism of the catalytic system

The C@TiO_2-HNBs show very high photocatalytic properties.[46,47] We propose a possible photocatalytic mechanism, as shown in Fig. 9, which consists of two aspects, C doped and C coated TiO_2-HNBs. Based on the above analysis, it can be concluded that doped C mainly replaces Ti atoms in the surface lattice to form a carbonate structure. C doped into the lattice of TiO_2-HNBs resulted in doped carbon forming a C doping energy level above the valence band of TiO_2, which reduces the band gap of TiO_2. This results in the absorbance of more visible light and the generation of more electron–hole pairs, thereby increasing the photocatalytic capacity of the catalyst. Coated C is mainly in the form of graphite coated on the surface of TiO_2, which can provide more active sites and adsorb more active species. In addition, glucose molecules and graphite-like carbon species are types of electron donor molecule that capture holes in photogenerated electron–hole pairs. This in turn causes the electrons to be separated and undergo a series of chemical reactions to form hydroxyl radicals. Hydroxyl radicals degrade organic pollutants adsorbed on the catalyst surface. Whilst compiling this C doped and coated mechanism, we found that the amount of C doped and coated should not be too much. If the amount of coated C is too large, it can easily lead to catalyst agglomeration or defects in the catalyst surface, which can become the recombination center of photo-generated electron–hole pairs.

4. Conclusions

A series of visible-light-driven photocatalysts, based on carbon doped and coated TiO_2 hollow nanocubes assembled using six ordered nanosheets with a dominant exposure of high energy {001} facets, were synthesized using facile one-step solvothermal treatment *via* a topotactic transformation process with $TiOF_2$ as a template and glucose as a carbon source. The morphology of the 3D hierarchical TiO_2 hollow nanocubes can be altered through systematic adjustment of the reaction time and glucose/$TiOF_2$ mass ratio. The results indicated that glucose not only provided the carbon source for doping and coating by dehydration reactions, but also played an important role in structure control during synthesis, by providing H_2O as the carbonization medium. Coated carbon was deposited predominantly on the surface as graphitic carbon in extended p conjugated graphite-like arrangements and doped carbon in the TiO_2 lattice dominantly occurred by substitution of Ti to form a carbonate structure. This was confirmed using XPS, FT-IR, DRS and Raman spectroscopic studies. The photocatalytic RhB degradation rate constant of the optimal catalyst, T24-0.15, is much larger (7.0 times) than that of the TiO_2-HNBs. This novel approach is expected to provide a perfect reference for the perfect combination of two modification methods, "surface sensitized" and "element doped", to synergistically fabricate other carbon-material-based TiO_2 composites, which is of great value with promising application.

Conflicts of interest

There are no conflicts to declare.

Acknowledgements

The authors would like to thank the National Natural Science Foundation of China (20702064, 21177161 and 31402137), the Science Foundation of Hubei Province for Distinguished Young Scholars (2013CFA034) and the Program for Excellent Talents in Hubei Province (RCJH15001) for support, funded by the Opening Project of Key Laboratory of Green Catalysis of Sichuan Institutes of High Education (LYZ1107) and the Fundamental Research Funds for the Central University, South-Central University for Nationalities (CZP17077).

References

1 K. Yang, Y. Dai, B. Huang and M. H. Whangbo, Density functional characterization of the visible-light absorption in substitutional C anion and C-cation-doped TiO_2, *J. Phys. Chem. C*, 2009, **113**, 2624–2629.

2 C. Dette, M. A. Perez-Osorio, C. S. Kley, P. Punke, C. E. Patrick, P. Jacobson, F. Giustino, S. J. Jung and K. Kern, TiO_2 anatase with a bandgap in the visible region, *Nano Lett.*, 2014, **14**, 6533–6538.

3 J. Dong, J. Han, Y. Liu, A. Nakajima, S. Matsushita, S. Wei and W. Gao, Defective black TiO_2 synthesized *via* anodization for visible light photocatalysis, *ACS Appl. Mater. Interfaces*, 2014, **6**, 1385–1388.

4 C. Zha, L. Shen, X. Zhang, Y. Wang, B. A. Korgel, A. Gupta and N. Bao, Double-sided brush-shaped TiO_2 nanostructure assemblies with highly ordered nanowires for dye-sensitized solar cells, *ACS Appl. Mater. Interfaces*, 2014, **6**, 122–129.

5 R. J. Braham and A. T. Harris, Review of major design and scale-up considerations for solar photocatalytic reactors, *Ind. Eng. Chem. Res.*, 2009, **48**, 8890–8905.

6 J. Zhang, Y. Wu, M. Xing, S. A. K. Leghari and S. Sajjad, Development of modified N-doped TiO_2 photocatalyst with metals, nonmetals and metal oxides, *Energy Environ. Sci.*, 2010, **3**, 715–726.

7 D. Chen, Z. Jiang, J. Geng, Q. Wang and D. Yang, Carbon and nitrogen co-doped TiO_2 with enhanced visible-light photocatalytic activity, *Ind. Eng. Chem. Res.*, 2007, **46**, 2741–2746.

8 H. G. Yang, C. H. Sun, S. Z. Qiao, J. Zou, G. Liu, S. C. Smith, H. M. Cheng and G. Q. Lu, Anatase TiO_2 single crystals with a large percentage of reactive facets, *Nature*, 2008, **453**, 638.

9 G. Liu, J. C. Yu, G. Q. Lu and H. M. Cheng, Crystal facet engineering of semiconductor photocatalysts: motivations, advances and unique properties, *Chem. Commun.*, 2011, **47**, 6763–6783.

10 K. L. Lv, B. Cheng, J. G. Yu and G. Liu, Fluorine ions-mediated morphology control of anatase TiO_2 with enhanced photocatalytic activity, *Phys. Chem. Chem. Phys.*, 2012, **14**, 5349–5362.

11 X. G. Han, Q. Kuang, M. S. Jin, Z. X. Xie and L. S. Zheng, Synthesis of Titania nanosheets with a high percentage of exposed (001) facets and related photocatalytic properties, *J. Am. Chem. Soc.*, 2009, **131**, 3152–3153.

12 C. Sushmaa and S. Girish Kumar, C-N-S tridoping into TiO_2 matrix for photocatalytic applications: observations, speculations and contradictions in the codoping process, *Inorg. Chem. Front.*, 2017, **4**, 1250–1267.

13 C. Lin, Y. Song, L. Cao and S. Chen, Effective photocatalysis of functional nanocomposites based on carbon and TiO_2 nanoparticles, *Nanoscale*, 2013, **5**, 4986–4992.

14 J. Zhong, F. Chen and J. Zhang, Carbon-deposited TiO_2: synthesis, characterization, and visible photocatalytic performance, *J. Phys. Chem. C*, 2010, **114**, 933–939.

15 Q. Xiang, J. Yu and M. Jaroniec, Enhanced photocatalytic H_2 production activity of graphene-modified titania nanosheets, *Nanoscale*, 2011, **3**, 3670–3678.

16 S. Shanmugam, A. Gabashvili, D. S. Jacob, J. C. Yu and A. Gedanken, Synthesis and characterization of TiO_2@C core-shell composite nanoparticles and evaluation of their photocatalytic activities, *Chem. Mater.*, 2006, **18**, 2275–2282.

17 F. Zuo, K. Bozhilov, R. J. Dillon, L. Wang, P. Smith, X. Zhao, C. Bardeen and P. Feng, Active Facets on Titanium(III)-Doped TiO_2: an effective strategy to improve the visible light photocatalytic activity, *Angew. Chem.*, 2012, **124**, 6327–6330.

18 Z. J. Wang, M. Liu, G. J. Wei, P. Han, X. X. Zhao, J. X. Liu, Y. Zhou and J. Zhang, Hierarchical self-supported C@TiO_2-MoS2 core-shell nanofiber mats as flexible anode for advanced lithium ion batteries, *Appl. Surf. Sci.*, 2017, **423**, 375–382.

19 L. Y. Hu, Y. M. Zhang, S. M. Zhang and B. X. Li, Transparent TiO_2-C@TiO_2-graphene free-standing film with enhanced visible light photocatalysis, *RSC. Adv.*, 2014, **2**, 43098–43103.

20 L. Zhang, M. S. Tse, O. K. Tan, Y. X. Wang and M. Han, Facile fabrication and characterization of multi-type carbon-doped TiO_2 for visible light-activated photocatalytic mineralization of gaseous toluene, *J. Mater. Chem. A.*, 2013, **1**, 4497–4507.

21 S. Wang, L. Zhao, L. Bai, J. Yan, Q. Jiang and J. Lian, Enhancing photocatalytic activity of disorder engineered C/TiO_2 and TiO_2 nanoparticles, *J. Mater. Chem. A.*, 2014, **2**, 7439–7445.

22 R. Kaplan, Review: Pharmacological pollution in water, *Crit. Rev. Environ. Sci. Technol.*, 2013, **43**, 1074–1116.

23 J. Sun, X. Yan, K. L. Lv, S. Sun, K. J. Deng and D. Y. Du, Enhancement of catalytic degradation of Rhodamine B under sunlight with Au loading TiO_2 nanotube arrays, *J. Mol. Catal. A: Chem.*, 2013, **367**, 31–37.

24 A. Fujishima, T. N. Rao and D. A. Tryk, Titanium dioxide photocatalysis, *J. Photochem. Photobiol., C*, 2000, **1**, 1–21.

25 D. Avisar, I. Horovitz, L. Lozzi, F. Ruggieri, M. Baker, M. L. Abel and H. Mamane, Impact of water quality on removal of carbamazepine in natural waters by N-doped TiO_2 photocatalytic thin film surfaces, *J. Hazard. Mater.*, 2012, **244–245**, 463–471.

26 M. Lazzeri, A. Vittadini and A. Selloni, Structure and energetics of stoichiometric TiO_2 anatase surfaces, *Phys. Rev. B: Condens. Matter Mater. Phys.*, 2001, **63**, 155409.

27 X. Han, Q. Kuang, M. Jin, Z. Xie and L. Zheng, Synthesis of titania nanosheets with a high percentage of exposed (001)

facets and related photocatalytic properties, *J. Am. Chem. Soc.*, 2009, **131**, 3152–3153.

28 S. Liu, J. Yu and M. Jaroniec, Anatase TiO_2 with dominant high energy {001} facets: Synthesis, properties, and applications, *Chem. Mater.*, 2011, **23**, 4085–4093.

29 W. J. Lee and Y. M. Sung, Synthesis of anatase nanosheets with exposed (001) facets *via* chemical vapor deposition, *Cryst. Growth Des.*, 2012, **12**, 5792–5795.

30 Z. Y. Wang, K. L. Lv, G. H. Wang, K. J. Deng and D. G. Tang, Study on the shape control and photocatalytic activity of high-energy anatase titania, *ACS Appl. Mater. Interfaces*, 2013, **5**, 8663–8669.

31 Y. M. Foong, A. T. T. Koh, H. Y. Ng and D. H. C. Chua, Mechanism behind the surface evolution and microstructure changes of laser fabricated nanostructured carbon composite, *J. Appl. Phys.*, 2011, **110**, 054904.

32 C. Z. Wen, Q. H. Hu, Y. N. Guo, X. Q. Gong, S. Z. Qiao and H. G. Yang, From titanium oxydifluoride ($TiOF_2$) to titania (TiO_2): Phase transition and non-metal doping with enhanced photocatalytic hydrogen (H_2) evolution properties, *Chem. Commun.*, 2011, **47**, 6138–6140.

33 M. Jung Jung, Y. Kim and Y. Seak Lee, Enhancement of the electrochemical capacitance of $TiOF_2$ obtained *via* control of the crystal structure, *J. Ind. Eng. Chem.*, 2017, **47**, 187–193.

34 Z. Hu, Z. Yan, P. K. Shen and C. J. Zhong, Nano-architectures of ordered hollow carbon spheres filled with carbon webs by template free controllable synthesis, *Nanotechnology*, 2012, **23**, 485404.

35 Y. Wang, R. Shi, J. Lin and Y. Zhu, Significant photocatalytic enhancement in methylene blue degradation of TiO_2 photocatalysts *via* graphene-like carbon in situ hybridization, *Appl. Catal., B*, 2010, **100**, 179–183.

36 X. Zhao, Y. T. Du, C. J. Zhang, L. J. Tian, X. F. Li, K. J. Deng, L. Q. Chen, Y. Y. Duan and K. L. Lv, Enhanced visible photocatalytic activity of TiO_2 hollow boxes modified by methionine for RhB degradation and NO oxidation, *Chin. J. Catal.*, 2018, **39**, 736–746.

37 Z. Y. Wang, B. B. Huang, Y. Dai, X. L. Zhu, Y. Y. Liu, X. Y. Zhang and X. Y. Qin, The roles of growth conditions on the topotactic transformation from $TiOF_2$ nanocubes to 3D hierarchical TiO_2 nanoboxes, *CrystEngComm*, 2013, **15**, 3436–3441.

38 S. F. Xie, X. G. Han, Q. Kuang, J. Fu, L. Zhang, Z. X. Xie and L. S. Zheng, Solid state precursor strategy for synthesizing hollow TiO_2 boxes with a high percentage of reactive {001} facets exposed, *Chem. Commun.*, 2011, **47**, 6722–6724.

39 J. Cai, Z. Wang, K. Lv, Y. Zheng, J. Yu and M. Li, Rapid synthesis of a TiO_2 hollow microsphere assembly from hollow nanoparticles with enhanced photocatalytic activity, *RSC Adv.*, 2013, **3**, 15273–15281.

40 N. Liu, H. Mirabolghasemi, K. Lee, S. P. Albu, A. Tighineanu, M. Altomare and P. Schmuk, Anodic TiO_2 nanotubes: double walled vs single walled, *Faraday Discuss.*, 2013, **164**, 107–116.

41 T. Li, B. Tian, J. Zhang, R. Dong, T. Wang and F. Yang, Facile tailoring of anatase TiO_2 morphology by use of H_2O_2: from microflowers with dominant {101} facets to microspheres with exposed {001} facets, *Ind. Eng. Chem. Res.*, 2013, **52**, 6704–6712.

42 R. Roy, Y. Sohn and D. Pradhan, Synergy of low-energy {101} and high-energy {001} TiO_2 crystal facets for enhanced photocatalysis, *ACS Nano*, 2013, **7**, 2532–2540.

43 M. V. Dozzi and E. Selli, Specific facets-dominated anatase TiO_2: fluorine-mediated synthesis and photoactivity, *Catalysts.*, 2013, **3**, 455–485.

44 S. Girish Kumar and K. S. R. Koteswara Rao, Polymorphic phase transition among the titania crystal structures using a solution-based approach: from precursor chemistry to nucleation process, *Nanoscale*, 2014, **6**, 11574–11632.

45 G. Liu, J. Pan, Y. Yang and M. Lu, Titanium dioxide crystals with tailored facets, *Chem. Rev.*, 2014, **114**, 9559–9612.

46 P. Zhang, T. Tachikawa, M. Fujitsuka and T. Majima, In situ fluorine doping of TiO_2 superstructures for efficient visible-light driven hydrogen generation, *ChemSusChem*, 2016, **9**, 617–623.

47 Y. Park, W. Kim, H. Park, T. Tachikawa, T. Majima and W. Y. Cho, Carbon-doped TiO_2 photocatalyst synthesized without using an external carbon precursor and the visible light activity, *Appl. Catal., B*, 2009, **91**, 355–361.